ELSEVIER

Journal of Photochemistry and Photobiology
A: Chemistry 85 (1995) 69–75

Journal of
PHOTOCHEMISTRY
AND
PHOTOBIOLOGY
A:CHEMISTRY

Mechanism of proton transfer in proteins II. Relationship between local properties of solvent and rate of excited state proton transfer for 2-naphthol derivatives bound to selected sites of proteins

Andrzej Jankowski[a], Wieslaw Wiczk[b], Tadeusz Janiak[b]

[a]*Institute of Chemistry, University of Wroclaw, F. Joliot-Curie 14, 50-383 Wroclaw, Poland*
[b]*Gdansk University, Department of Chemistry, Sobieskiego 18, 80-952 Gdansk, Poland*

Received 10 January 1994; accepted 19 May 1994

Abstract

Centres of gravity (CGs) of the fluorescence bands of protonated and deprotonated forms of 2-naphthol derivatives (NSOH), bound to proteins, were determined at various experimental conditions. CGs are correlated with the solvent relaxation time around fluorophores. The variation in the rate of excited state proton transfer (ESPT) for NSOH groups bound to proteins can be explained in terms of the solvent polarizability and the solvent relaxation rate with respect to a moving proton. From a comparison of the fluorescence decay data with the results of steady state measurements, the probability of geminal recombination in the ESPT reaction is estimated. This probability is negligible for one of our samples and 0.3–0.4 for two other samples. The mechanism of this effect is discussed briefly.

Keywords: Proton transfer; Proteins

1. Introduction

The transfer of a proton to water, which plays an important role in many biological processes, depends on the local structure of water around a proton donor group [1,2]. From X-ray diffraction and dielectric dispersion data, it is known that there are at least two modes of binding of water to proteins with markedly different physical properties from those of bulk water [3,4]. Therefore it can be inferred that the rate and mechanism of proton transfer in proteins may vary with the localization of the proton donor group within the protein macromolecule.

In previous work [5], we have studied the relationship between the electrostatic charge density and equilibrium and the rate constants of excited state proton transfer (ESPT) for 2-naphthol-6-sulphonic acid (NSOH) derivatives bound to proteins. In the present work, the relationship between the positions of the fluorescence bands of the NSOH groups bound to proteins and the rate of ESPT ($\tilde{k}_{pt}$) is investigated. We assume that the energy of solvent reorganization around excited fluorophores (Λ) is correlated with the maximum of the fluorescence band (Stokes shift [2]).

Information on the dynamics of solvent relaxation around fluorophores is also contained in the red edge effect. This effect involves a red shift of the centre of gravity of the fluorescence band on the frequency (ν) scale on excitation of a sample within the red edge of its absorption spectrum (ν_{edge}^{CG}) relative to the emission band excited normally near the absorption maximum (ν_{n}^{CG}). This occurs when the solvent relaxation time is comparable with the fluorescence lifetime.

The relationship between the red edge effect expressed as ($\nu_{n}^{CG} - \nu_{edge}^{CG}$), the dipolar relaxation time (τ_D) and the fluorescence lifetime (τ_f) is given by Bakhshiev [6,7] and Demchenko [8]. From the red edge effect, information may be obtained on the relaxation rate of the medium as a function of a change in dipole moment of a fluorescent compound on excitation. It can be assumed that the relaxation of the medium with respect to the movement of a proton will be correlated with the relaxation with respect to excitation.

We have studied the positions of the fluorescence bands of NSOH groups bound to selected sites of

SSDI 1010-6030(94)03885-X

proteins at excitation wavelengths near the maximum or within the red edge of the absorption band and at different pH values such that the ESPT reaction is present or eliminated. These results were correlated with the rate constants of ESPT. This correlation provided conclusions on the influence of the localization of the NSOH groups in the protein macromolecule on the mechanism of proton transfer. The time decay of the fluorescence of NSOH groups bound to proteins was also studied. A comparison of these results with steady state fluorescence data provided an estimation of the probability of the proton produced by ESPT to leave the solvent cage.

2. Experimental details

2.1. Materials

The following samples, described in detail in Ref. [9], were investigated: (a) papain labelled at the active site (cys 25) (PAP-NSOH); (b) bovine serum albumin (BSA) labelled preferentially at the surface of the molecule (BSA-NSOH(S)); (c) BSA with surface amino groups modified by phenylalanine to which NSOH groups were bound (BSAK); (d) BSA labelled preferentially in the hydrophobic interior of the molecule (BSA-NSOH(I)); (e) bromelain labelled analogously as PAP-NSOH (BRO-NSOH). Bromelain from Enzymes Ltd. (USA) contained some impurity and showed considerable absorbance at 320 nm (used for excitation of the fluorescence). Therefore the commercial preparation was purified by ion exchange chromatography before modification.

2.2. Methods

The absorption spectra were recorded and processed as described elsewhere [5]. The fluorescence spectra were recorded on a Perkin–Elmer (USA) model 204 instrument or on an SF1 module spectrofluorometer (Cobrabid-Optel, Poland), interfaced to a computer for control of measurements and storage and processing of the data. Fluorescence spectra of NSOH derivatives undergoing ESPT show two bands associated with protonated (ROH*, Scheme 1) and deprotonated (RO^-*) forms of the fluorophore.

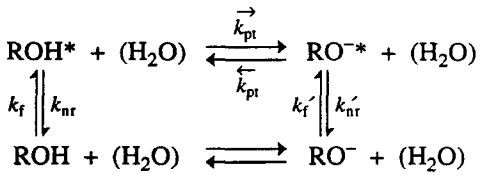

Scheme 1.

The fluorescence spectra had to be separated into component bands before determination of the band positions. This was performed using two methods, both based on the assumption that the contribution of individual species (ROH*, RO^-*) to the fluorescence intensity at a given wavelength at any solution pH is proportional to the fluorescence intensity of the same form at the same wavelength at a pH value at which the pure emission band of this form can be observed. In the first method, the spectra recorded on a Perkin–Elmer instrument were separated by the procedure described in Ref. [10]. In this procedure it is assumed that the error in separation is largest for wavelengths between the two separated bands because of the non-ideal resolution of the instrument. In the second method, the fluorescence spectra recorded on a Cobrabid-Optel apparatus and corrected for detector response [11] were separated by a simple simulation procedure assuming equal error probability over the whole wavelength range where fluorescence is observed. In both methods it is assumed that, in the presence of ESPT where both bands are visible, the position of the bands may be shifted with respect to those observed at pH values where only one form fluoresces because of the decrease in the excited state lifetime. The second method is more objective, but the systematic error due to non-ideal resolution is probably larger than in the first method.

The centre of gravity of the fluorescence bands was determined using [6,8,11]

$$\nu_{cg} = \int F_\nu \nu \, d\nu / \int F_\nu \, d\nu \ (cm^{-1}) \quad (1)$$

where F_ν is the fluorescence intensity at a given frequency of light. Shifts of ν_{cg} due to the red edge effect were determined by a change in excitation wavelength from 320 to 343 nm (31 250, 29 197 cm^{-1}) for the ROH* form and from 320 to 367 nm (31 250, 27 248 cm^{-1}) for direct excitation of the RO^- form.

Fluorescence decays were studied using an impulse fluorometer (Edinburgh Analytical Instruments, model CD-900) supplied with a hydrogen lamp (pulse width, 1 ns) by the single-photon-counting method. Analysis of the decay curves was performed according to the two-state excited state reaction model of Laws and Brand [12] expressed by (see also Ref. [13])

$$F(ROH^*) = \alpha_1 e^{-t/\tau_1} + \alpha_2 e^{-t/\tau_2} \quad (2)$$

$$F(RO^-{}^*) = \beta_1 e^{-t/\tau_1} + \beta_2 e^{-t/\tau_2} \quad (3)$$

It follows from this model that the fluorescence decay of our samples where ESPT takes place, observed at wavelengths at which the ROH* (Λ_1) or RO^-* (Λ_2) form emits, should be characterized by the same lifetime values (τ_1, τ_2) and definite amplitude values (α_1, α_2, β_1, β_2) [14]. The lifetimes and amplitudes found at various pH values and two wavelengths (Λ_1, Λ_2) were compared with the above model. The ESPT rate con-

stants ($\vec{k}_{pt}$) were determined from the difference between the reciprocals of the two lifetimes

$$\vec{k}_{pt} = 1/\tau_1 - 1/\tau_2 \quad (4)$$

where $\tau_1 = 1/(k_f + k_{nr} + \vec{k}_{pt})$ is the fluorescence lifetime of the ROH* form occurring at about pH 6 in the presence of ESPT and $\tau_2 = 1/(k_f + k_{nr})$ is the lifetime measured at near pH 0 in the absence of ESPT.

A comparison of the $\vec{k}_{pt}$ values obtained from fluorescence decay and steady state fluorescence measurements [5,9] allows an estimation to be made of the probability of geminal recombination (η) in the ESPT reaction. It has been shown [14,15] that, for some fluorophores with a strong negative electric charge, there is a probability of proton recombination within the excited state lifetime before leaving the solvent cage. In this case, the steady state concentration of the ROH* form (Scheme 1) will be higher and the RO^-* concentration lower than that obtained from time-resolved measurements.

By reasoning analogous to that of Weller [16], Eqs. (5) and (6) are obtained (see also Ref. [17])

$$\Phi_c/\Phi_0 = 1/[1 + \vec{k}_{pt}(1-\eta)\tau_0] \quad (5)$$

$$(1-\eta) = \frac{1 - \Phi_c/\Phi_0}{\Phi_c/\Phi_0(\vec{k}_{pt}\tau_0)} \quad (6)$$

where Φ_c and Φ_0 are the relative fluorescence quantum yields at pH 6 (in the presence of ESPT at $[H^+] \to 0$) and $pH < pK_a^*$ respectively, τ_0 is the fluorescence lifetime of the ROH* form in the absence of ESPT and η is the probability of geminal recombination

$$\eta = k_{GR}[RO_{sc}^-*]/\vec{k}_{pt}[ROH^*]$$

where $k_{GR}[RO_{sc}^-*]$ is the rate of geminal recombination (see Ref. [15]) and the subscript sc refers to the concentration of the RO^-* form within the solvent cage.

3. Results and discussion

3.1. Relationship between rate of ESPT and position of fluorescence band

The characteristics of the samples investigated are given in Table 1. The fluorescence spectrum of a protein modified by NSOH groups, separated into the ROH* and RO^-* component bands by the second method (see Section 2), is shown in Fig. 1.

The differences between the maxima of the absorption (gaussian) bands and the centres of gravity of the fluorescence bands (Stokes shifts) are given in Table 2. There seems to be no correlation between the Stokes shifts and the $\vec{k}_{pt}$ values.

The influence of the excitation wavelength and pH on the centres of gravity of the ROH* and RO^-* fluorescence bands separated by the second method is shown in Table 3. The results obtained by the first method (not shown) are essentially convergent with those of Table 3. The fluorescence bands of the ROH* form at pH 0 (in the absence of ESPT) are centred at lower electromagnetic wave energy compared with analogous bands observed in the presence of ESPT at pH 6. This may be due to favourable emission from fluorophores which are less relaxed with respect to the solvent in the presence of ESPT (lower lifetime). However, the centres of gravity of the ROH* bands obtained at pH 0 are questionable because of the possible unfolding of the protein which can influence the position of the emission bands.

The red edge effect is expressed as the difference between the centre of gravity of the fluorescence band excited near the absorption maximum (ν_{320}) and that excited at the red edge of the absorption band (ν_{edge}). The red edge effect for the ROH* form at pH 6 is higher for BSA-NSOH(S) than for BSAK. Such a high red edge effect for BSA-NSOH(S) is unexpected for fluorophores with high accessibility to water (see Table 1). It may be due to the short connection between the

Table 1
Characteristics of NSOH groups in the samples investigated

Sample	Accessibility to water[a]	Number of NSOH groups per protein molecule[a]	Φ_0[b]	Φ_0'[b]	pK_a[c]	pK_a^*[c]
BSAK	0.62	17.0	0.16	0.28	11.1	1.37
BSA-NSOH(S)	0.74	0.8	0.11	0.17	9.3	0.3
PAP-NSOH	0.33	1.1	0.05	0.10	8.7	−0.26
BRO-NSOH	0.40	1.2		0.11		
BSA-NSOH(I)	0.30	39.0	0.03	0.13	9.7	0.4
Phe-NSOH	1.0	–	0.25	0.50	9.2	0.6

[a]From Ref. [9].

[b]Φ_0 and Φ_0' are the fluorescence quantum yields of ROH* and RO^-* forms at $pH < pK_a^*$ and $pH \gg pK_a$ respectively.

[c]pK_a and pK_a^* are the negative logarithms of the equilibrium constants of proton transfer in the ground and excited states respectively.

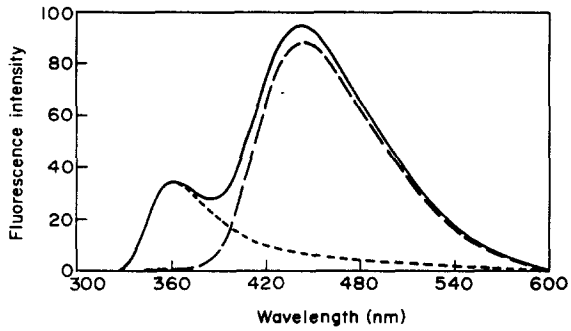

Fig. 1. Corrected fluorescence spectrum of BSAK at pH 6 excited at 320 nm. ——, Experimental results; – – –, RO^-* contribution; -----, ROH* contribution.

Table 2
Differences between the maxima of the absorption and fluorescence bands (Stokes shifts) for NSOH groups bound to proteins

Sample	Positions of band maxima (cm^{-1})				Stokes shift (cm^{-1})		$\vec{k}_{pt}$* ($\times 10^{-8}$)
	Absorption		Fluorescence		ROH*	RO^{-}*	
	ROH*	RO^{-}*	ROH*	RO^{-}*			
BSAK	33300	28300	26123	22275	7177	6025	4.560
BSA-NSOH(S)	33300	28600	26608	22338	6692	6262	1.847
PAP-NSOH	33300	28500	26133	21783	7167	6717	19.625
BSA-NSOH(I)	33300	28600	25512	22311	7788	6289	10.4
Phe-NSOH	33513	29061	26860	22841	6653	6220	12.1

*Results calculated from steady state fluorescence measurements (see Ref. [9]).

Table 3
Centres of gravity (CGs) of the fluorescence bands of NSOH groups bound to proteins

Sample	CG of ROH* form (cm^{-1})		Red edge effect (cm^{-1})	CG of RO^{-}* form (cm^{-1})		Red edge effect (cm^{-1})
	λ_{exc} = 320 nm	λ_{exc} = 343 nm		λ_{exc} = 320 nm	λ_{exc} = 343 or 367 nm	
BSAK						
pH 0	26123	25420	703			
pH 6	26228	26123	165	22047	22072	−25
pH 11				22276	22254	22
BSA-NSOH(S)						
pH 0	26608	26150	458			
pH 6	26828	26368	460	22218	22596	−378
pH 11				23338	23354	−16
PAP-NSOH						
pH 0	26133					
pH 6	26348			22111	21889	222
pH 11				21783	21386	397
BSA-NSOH(I)						
pH 0	25512					
pH 6	25995			22161		
pH 11				22312		
Phe-NSOH						
pH 6	26860	26865	5			

NSOH groups and the protein and/or to partial shielding of the fluorophores from the solvent which is not detected by our method of determination of the accessibility. The higher red edge effect indicates that the solvent relaxation around excited fluorophores is slower for BSA-NSOH(S) than for BSAK. For PAP-NSOH, the red edge effect of the ROH* form could not be measured because of the low fluorescence intensity and the contribution from scattered light on excitation at 343 nm. For Phe-NSOH (low molecular weight analogue of NSOH groups), practically no red edge effect was observed (Table 3).

A comparison of the red edge effects ($\nu_{320} - \nu_{edge}$) for the ROH* fluorescence bands of BSAK and BSA-NSOH(S) (Table 3) with the $\vec{k}_{pt}$ values (Table 2) suggests that an increase in the solvent relaxation rate, which is inversely proportional to ($\nu_{320} - \nu_{edge}$) [6–8], contributes to the enhancement of the rate of ESPT.

The red edge effect for the RO^{-}* band on excitation of the ROH form at pH 6, is easier to observe than that of the ROH* band because of the larger spectral distance between the red edge excitation and observation wavelengths. However, there are some difficulties in interpretation due to contamination of effects associated with a change in dipole moment of the NSOH group on excitation and on charge separation by proton transfer. Therefore no quantitative conclusions are possible.

For some samples, the RO^{-}* band shows a negative red edge effect. This phenomenon requires some explanation. Excitation of a sample at the red edge of its spectrum favours light absorption by those fluorophores which are less relaxed in the ground state and

more relaxed in the excited state with respect to the local structure of the solvent [6,8,11]. If solvent relaxation is not complete before emission (τ_D comparable with τ_f), the preference for excitation of the fluorophores at the lowest absorbed energy (red edge) is "remembered" in the excited state. The centre of gravity of the fluorescence band excited at the red edge is positioned at a lower frequency than that excited near the absorption maximum. However, if the ROH form is excited and emission from the RO^{-}* species formed after excitation is observed, it is possible that the molecules which are less relaxed in the ground state and more relaxed in the excited state in the ROH form will behave oppositely in the RO^{-}* form, showing a centre of gravity of the fluorescence band excited at the red edge of the absorption spectrum at a higher energy than that excited near the centre of the absorption band, i.e. a negative red edge effect ($\nu_{320} < \nu_{edge}$). Such a situation occurs if the direction of solvent polarization induced by excitation is reversed by subsequent proton transfer (see Scheme 2). Such an effect is observed for BSA-NSOH(S) and BSAK, although in the former case it is more negative (Table 3). This suggests that, for BSA-NSOH(S), there is a greater difference, relative to BSAK, between the orientation of the solvent molecules in the ROH* and RO^{-}* forms.

For PAP-NSOH, the red edge effect of the RO^{-}* band is positive, suggesting that, in this case, the direction of the polarization vector for the ROH* and RO^{-}* forms is similar. A negative red edge effect is observed because of the opposite direction of the polarization vector in Scheme 2. Obviously, reversal of the polarization direction enhances the reaction barrier for ESPT and lowers the $\vec{k}_{pt}$ value. From a thermodynamic point of view, this effect is described as a decrease in the ESPT rate caused by an increase in the energy of outer sphere reorganization by proton transfer (Λ_{out}, see Refs. [2,5]). The molecular environment of NSOH groups bound to proteins may affect the solvent polarizability by changing the water structure or by additional polarization by nearby charged groups of the protein. This latter effect may occur in papain containing Asp and His residues [18] near to bound NSOH groups. Such an effect can decrease the polarization changes by ESPT and enhance the $\vec{k}_{pt}$ value for PAP-NSOH.

Another explanation [9] for the elevated $\vec{k}_{pt}$ values for NSOH groups bound inside macromolecules, which assumes that the polarization of the solvent in the hydrophobic core of a protein is too slow to follow the movement of a proton, seems to be unlikely for the following reasons. The absolute value of the red edge effect ($\nu_{320} - \nu_{edge}$) for the RO^{-}* form of BSAK (Table 3) is lower than those for PAP-NSOH and BSA-NSOH(S), which are comparable. (The value of the red edge effect for BSAK at pH 0 is rejected as doubtful (see above).) It can be supposed that if the red edge effect for the ROH* band could be measured for PAP-NSOH, it would be comparable with that for BSA-NSOH(S). We conclude that the increase in $\vec{k}_{pt}$ for our samples is not proportional to the decrease in ($\nu_{320} - \nu_{edge}$) treated as a measure of the relaxation time (τ_D). Therefore the conclusion given above, based on the comparison of the red edge effects for the ROH* forms of BSAK and BSA-NSOH(S), should be modified as follows. A decrease in $\vec{k}_{pt}$ with a change in environment of the NSOH groups in the protein molecule may be caused not only by a decrease in the rate of solvent relaxation, but also by the reversal of the solvent polarization vector by proton transfer as in the case of BSA-NSOH(S).

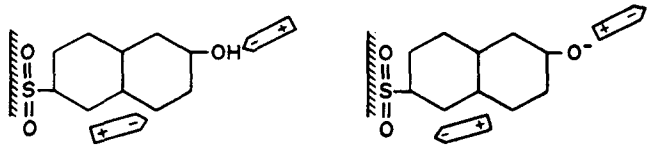

Scheme 2.

3.2. Time decay of emission intensity of NSOH groups bound to proteins

An emission decay curve for a protein-NSOH conjugate is shown in Fig. 2. The amplitudes, lifetimes and $\vec{k}_{pt}$ values obtained using the decay data are shown in Tables 4 and 5. For fluorophores bound to selected sites of macromolecules, non-exponential decay of each form (ROH*, RO^{-}*) can be anticipated because of the inhomogeneity of the medium and the dynamic disorder of the environment [19]. Fits of our decay data to double or triple exponential models seem satisfactory in most cases. We attempted to ascribe particular lifetimes to the ROH* and RO^{-}* forms of our samples using the Laws and Brand model of ESPT [12,13]. It follows from this model that the decay of the ROH* form, observed at 365 nm at $pH < pK_a$*, should be monoexponential with an amplitude α_2 and lifetime τ_2 (Eqs. (2) and (3)), and at pH 6, at an $[H^+]$ concentration near to zero, monoexponential but with amplitude α_1 and lifetime τ_1. The decay of the RO^{-}* form observed at 445 nm at pH 6 should be biexponential with amplitudes $\beta_2 = -\beta_1$ and lifetimes τ_1 and τ_2.

From Fig. 1, the decay of RO^{-}* is visible at 445 nm; the contribution of fluorescence from the ROH* form is non-negligible. Because of this and due to the presence of some additional decay components (τ_3, α_3, Table 4), the amplitudes given in Table 4 cannot always be reconciled with the model of Laws and Brand [12]. The lifetimes in Table 4 seem to correlate with the ESPT model if some values are rejected. The criterion for rejection was the assumption that the lifetimes of NSOH groups bound to proteins cannot be higher than

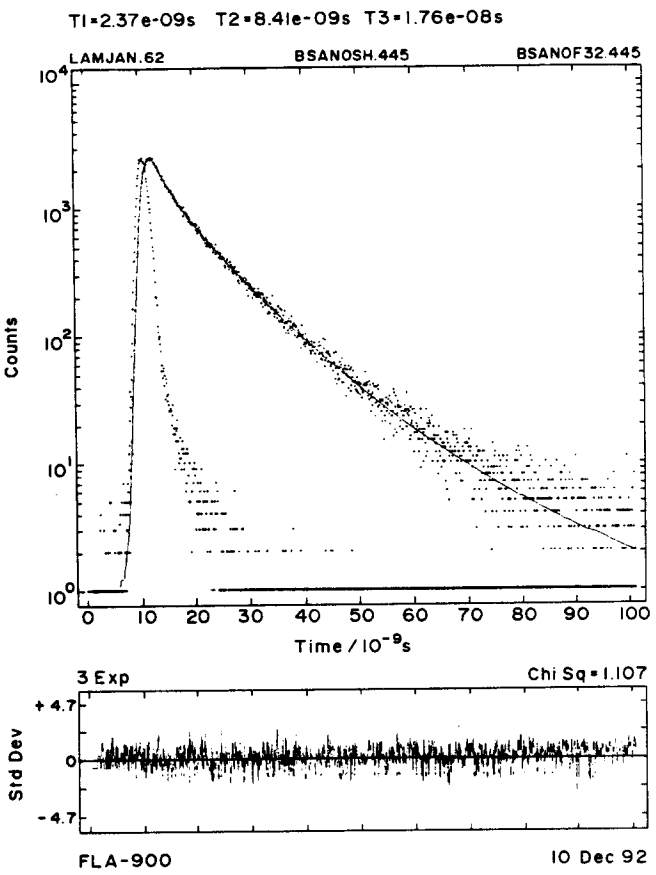

Fig. 2. Fluorescence decay of BSA-NSOH(S) at pH 6 observed at 443 nm.

that for Phe-NSOH (low molecular weight analogue of NSOH) for which the fluorescence quantum yield is higher. Using this assumption, the remaining lifetimes can be ascribed to ROH* and RO^{-}* decays according to the above model. Only those decay curves for which χ^2 was less than two were taken into account. The $\vec{k}_{pt}$ values calculated from the decay data (Eq. (5)) are given in Table 5. Two facts support our lifetime assignments and $\vec{k}_{pt}$ calculations: (a) the τ_2 values are roughly proportional to the fluorescence quantum yields (Φ_0, Φ_0') given in Table 1; (b) if the lifetimes of Table 5 are substituted into the equations $k_f = \Phi_0/\tau_2$ or $k_f = \Phi_c/\tau_1$ (where k_f is the fluorescence rate constant and Φ_0 and Φ_c are the fluorescence quantum yields of ROH* determined at pH 0 and pH 6 respectively), a similar result is obtained (Table 6).

The probability of geminal recombination (η), calculated from a comparison of the $\vec{k}_{pt}$ values obtained from decay data and steady state measurements (Eq. (6)), is given in Table 5. The value for BSAK is near to zero and for PAP-NSOH and BSA-NSOH(S) is lower than 0.5. Decay curves (Fig. 2) for PAP-NSOH, BRO-NSOH and BSA-NSOH(S) show "tails" at higher time intervals after the excitation pulse. Such an effect is thought to be characteristic of geminal recombination in ESPT [15,16]. Long lifetime components appearing in nearly all fits (Table 4) may also be due to geminal recombination.

4. Conclusions

It has been shown previously [9] that the rate of ESPT for NSOH groups bound to proteins varies markedly depending on the localization of the fluorophore in the macromolecule. In some cases, higher rate constants of ESPT were found for groups bound inside the hydrophobic core of the protein. This seems to contradict the simple diffusion control theory of ESPT. In this work, based on a study of the centres of gravity of the fluorescence bands of NSOH groups in proteins, it is concluded that the variation of the rate of ESPT with the localization of the fluorophore in the macromolecule is due to the immobilization of the water molecules near the protein surface (see Ref. [17]) and to changes in solvent polarizability dependent on the local environment of the proton donor. This is in accord with previous results [5].

The probability of geminal recombination in the ESPT reaction (η) also depends markedly on the position of

Table 4
Decay parameters for NSOH groups bound to proteins[a]

Sample	Observation (365 nm), pH 0				Observation (365 nm), pH 6				Observation (445 nm), pH 6					
	τ_2 (ns)	α_2	τ_1 (ns)	α_1	τ_2 (ns)	α_2	τ_1 (ns)	α_1	τ_2 (ns)	α_2	τ_1 (ns)	α_1	τ_3 (ns)	α_3
BSAK	5.81	0.03	2.92	0.04	5.77	0.02	1.74	0.08	5.12	0.02	1.50	−0.03	9.80	0.04
BSA-NSOH(S)	5.2[b]				8.06	0.03	1.92	0.05	8.41	0.03	2.37	0.03	17.6	0.003
PAP-NSOH	3.4[b]								9.03	0.02	2.81	0.01	19.6	0.001
BRO-NSOH									5.12	0.02	0.7	0.03	11.8	0.03
Phe-NSOH							7.17[b]		10.23[b]					

[a]Symbols are explained in Eqs. (2)–(4).
[b]From Ref. [5].

Table 5
Comparison of ESPT rate constants ($\bar{k}_{pt}$) calculated from fluorescence decays and steady state fluorescence measurements

Sample	τ_2[a] (ns)	τ_1[a] (ns)	$k_{pt}\times10^{-8}$ (Eq. (5))	Φ_c/Φ_0[b]	Φ'_c/Φ'_0[b]	$k_{pt}\tau_0$ steady state	Probability of geminal recombination (Eq. (6))
BSAK	6.42[c]	1.501	5.104	0.274	0.728	4.560	0.19
BSA-NSOH(S)	6.24[c]	2.374	2.609	0.51	0.464	1.847	0.41
PAP-NSOH	3.75[c]	0.35[d]	25.90	0.13	0.76	19.625	0.31

[a]Symbols explained in Eqs. (2)–(4).
[b]Symbols explained in Eqs. (5) and (6).
[c]Data of Table 4 corrected for quenching of ROH species by protons (see Ref. [12]) according to the method described in Ref. [9].
[d]Value of τ_1 for BRO-NSOH (analogue of PAP-NSOH), because of the analogy between the enzymes, was decreased by 50% assuming proportionality between the fluorescence quantum yield and lifetime.

Table 6
Fluorescence rate constants (k_{pt}) calculated from results obtained at pH 0 ($k_0=\Phi_0/\tau_2$) and pH 6 ($k_1=\Phi_c/\tau_1$)

Sample	τ_2 (ns)	Φ	$k\times10^{-7}$	τ_1 (ns)	Φ	$k\times10^{-7}$
BSAK	6.42	0.16	2.4922	1.501	0.0438	2.9226
BSA-NSOH(S)	6.24	0.11	1.7628	2.374	0.0561	2.3631
PAP-NSOH	3.75	0.05	1.3333	0.35	0.0065	1.8571

Symbols as in Tables 4 and 5.

the NSOH groups in the macromolecule. In some cases (BSA-NSOH(S)), increased η may be due to the influence of the surface charge density of the protein, and in other cases (PAP-NSOH), a mechanism described in Ref. [17] may apply. It is expected [20] that many biological processes dependent on proton gradients (see Refs. [9,17]) may be controlled by excitation of appropriately localized fluorescent probes showing ESPT. It is obvious that the biological efficiency of such a method would be limited by geminal recombination. Our results show that this effect, although considerable, does not exclude the possibility of using NSOH groups to create local proton gradients in biological systems. Further studies in this area are needed.

Acknowledgement

This work was supported by a Committee of Scientific Research (KBN-2.0760-91) grant.

References

[1] M. Gutman, D. Huppert and E. Nachliel, *Int. J. Biochem., 121* (1982) 637–642.
[2] R.A. Marcus, *J. Phys. Chem., 72* (1968) 891–899.
[3] P. Pissis, *J. Mol. Liq., 41* (1989) 277–289.
[4] W. Saenger, *Annu. Rev. Biophys. Chem., 16* (1987) 93–114.
[5] A. Jankowski and P. Stefanowicz, in press.
[6] N. Bakhshiev, *Izv. Akad. Nauk SSSR, 32* (1968) 1360–1370.
[7] J. Mazurenko and N. Bakhshiev, *Opt. Spectrosc. (SSSR), 28* (1970) 905–913.
[8] A. Demchenko, *Essays Biochem., 22* (1986) 120–157.
[9] A. Jankowski, P. Stefanowicz and P. Dobryszycki, *J. Photochem. Photobiol. A: Chem., 69* (1992) 57–66.
[10] A. Jankowski, I.Z. Siemion and Z. Szewczuk, *Acta Biochem. Polon., 28* (1981) 11–20.
[11] J.R. Lakowicz, *Principles of Fluorescence Spectroscopy*, Plenum, New York, 1983.
[12] W. Laws and L. Brand, *J. Phys. Chem., 83* (1979) 795–802.
[13] J.R. Lakowicz and A. Balter, *Biophys. Chem., 16* (1982) 223–240.
[14] H. Haar, U. Klein and M. Hauser, *Chem. Phys. Lett., 58* (1978) 525–530.
[15] E. Pines, D. Huppert and N. Agmon, *J. Chem. Phys., 86* (1988) 5620–5630.
[16] A. Weller, *Z. Elektrochem., 56* (1952) 662–667.
[17] M. Gutman and E. Nachliel, *Biochem. Biophys. Acta, 1015* (1990) 391–414.
[18] I. Kamphuis, J. Drength and E. Balus, *J. Mol. Biol., 182* (1985) 317–329.
[19] K. Sienicki, S. Blonski and G. Durocher, *J. Phys. Chem., 95* (1991) 1576–1579.
[20] J. Clark, S. Shapiro, P. Campillo and K. Winn, *J. Am. Chem. Soc., 101* (1979) 746–748.
[21] J.R. Lakowicz, *J. Biochem. Biophys. Methods, 2* (1980) 91–119.